scientific reports

Check for updates

OPEN

Proteomic signatures and mitochondrial dysfunctions in peripheral T cells reveal novel insights into Alzheimer's disease

Sebile Koca[1], Irem Kiris[2], Sevki Sahin[3], Sibel Karsidag[4], Nilgun Cinar[5] & Ahmet Tarik Baykal[6]✉

Alzheimer's disease (AD) exhibits progressive cognitive decline and recent scientific studies hint to the peripheral immune system as a contributor. In this study, we isolated peripheral immune cells including CD4 + and CD8 + T cells, CD14 + monocytes and CD19 + B cells from AD patients and age-matched controls via fluorescence-activated cell sorting. Label-free LC–MS/MS-based proteomic expression analysis within each cell type, comparing AD and control groups independently, 387 significantly altered proteins were identified in CD4 + and 121 in CD8 + T cells. Bioinformatic analysis uncovered distinct, cell-type-specific signatures: CD4 + cells showed dysregulation in ribosomal and RNA-binding proteins linked to neurodegeneration and oxidative stress while CD8 + cells showed elevated glycolytic enzyme expression and hyperpolarized mitochondrial membrane potential. Furthermore, mitochondrial functional assays, JC-1 and MitoSOX Red, further supported cell-type-dependent differences in mitochondrial activity. These findings may suggest that peripheral T cells have unique proteomic and functional alterations in AD, implicating mitochondrial dysfunction as a potential contributor to disease pathology.

Keywords Alzheimer's disease, CD4 + T cell, CD8 + T cell, LC–MS/MS, Oxidative stress, Mitochondrial membrane potential

Alzheimer's disease (AD) is the most prevalent form of dementia and characterized by progressive cognitive decline[1]. Although extensive research has been conducted, the pathological mechanisms of AD are still not fully understood. AD is neuropathologically defined by the accumulation of misfolded and aggregated amyloid-β peptides and phosphorylated tau[2]. AD is a brain disorder; however, it is shown to be transmissible by blood and stem cell implantation[3,4]. Furthermore, healthy blood transfusion reduced the pathological AD markers[5,6]. Therefore, to understand the underlying mechanism and the pathogenesis of AD, peripheral systems should be investigated along with the brain.

Recent findings highlight the importance of immune system dysregulation and mitochondrial dysfunction[7–10]. The peripheral immune system has a complex and dynamic role with different immune cell types influencing disease progression through diverse mechanisms[7,11]. Comprehensive understanding of peripheral immune cell alterations in AD requires cell-specific researches[12]. Although proteomic approaches provide an effective method for identifying disease-associated molecular signatures, most studies have focused primarily on plasma, serum, CSF, or peripheral blood mononuclear cells (PBMCs) with only limited research investigating cell-specific proteomic changes in different peripheral immune cells[13–16].

Mitochondrial dysfunction is closely associated with the progression of AD[9]. Structural and functional mitochondrial alterations, including changes in distribution, mobility, oxidative stress, enzyme disruptions,

[1]Department of Biochemistry and Molecular Biology, Institute of Health Sciences, Acibadem Mehmet Ali Aydinlar University, Istanbul, Türkiye. [2]Faculty of Engineering and Natural Sciences, Sabanci University, Istanbul, Türkiye. [3]Department of Neurology, Faculty of Medicine, University of Health Sciences, Sancaktepe Sehit Prof. Dr. Ilhan Varank Training and Research Hospital, Istanbul, Türkiye. [4]Department of Neurology, Faculty of Medicine, University of Health Sciences, Sultan 2. Abdulhamid Han Training and Research Hospital, Istanbul, Türkiye. [5]Department of Neurology, Faculty of Medicine, Maltepe University, Istanbul, Türkiye. [6]Department of Medical Biochemistry, Faculty of Medicine, Acibadem Mehmet Ali Aydinlar University, Icerenkoy Mh. No:32, Kayisdagi Cd, 34752 Atasehir, Istanbul, Turkey. ✉email: ahmet.baykal@acibadem.edu.tr

metabolic impairments, and reduced biogenesis, further support its critical role in AD progression[17]. In addition, recent studies indicate the role of peripheral mitochondrial dysfunction in AD[18,19]. Wang et al., 2020 presents the alterations of many mitochondrial proteins across the AD cortex, CSF, and serum. Another study conducted on PBMCs from Parkinson's disease patients identified increased mitochondrial dysfunction and oxidative stress, particularly in monocytes. They were also suggested that further studies on other neurodegenerative patient groups would help define PBMC pathology[20].

In our study, we performed LC–MS/MS analysis on CD4 + and CD8 + T cells, CD14 + monocytes, and CD19 + B cells from AD patients and control groups to investigate the specific effects of these cell subgroups on the disease mechanism in detail. Using JC-1 and MitoSOX Red assays, we quantified mitochondrial membrane potential (ΔΨm) and oxidative stress levels in these cell subgroups. Our study, focusing on proteome profile and mitochondrial changes, provides an insight into the role of peripheral immune cell subgroups, particularly in CD4 + and CD8 + T cells, in AD.

Materials and methods

Ethical statement

The research was approved by the Clinical Research Ethics Committee (ATADEK) at Acibadem Mehmet Ali Aydinlar University (No: 2016/8–34, Date: 12 May 2016) and complies with the guidelines of the Helsinki Declaration. A written informed consent was given by all participants who took part in this study.

AD diagnosis and collection of blood samples

The experimental and analysis workflow of the study is represented in Fig. 1. The study included all instances of AD that met the diagnostic criteria of "The National Institute of Neurologic, Communicative Disorders, and Stroke–AD and Related Disorders Association (NINCDS-ADRDA)"[21]. Moderate stage AD cases were selected based on the Clinical Dementia Rating (CDR) scale[22]. Additionally coginitive status was quantified using the Mini Mental State Examination (MMSE)[23]. Blood samples from 20 AD patients and 23 age-matched healthy controls were collected by venipuncture into sodium-heparin tubes from dementia clinic (Table 1). At the time of blood collection from healthy volunteers, there were no indications or diagnoses of cognitive or mental health disorders. Furthermore, they were also not taking any medications for neurological or psychiatric conditions. Two outlier AD samples were excluded from CD4 + subgroup after the LC–MS/MS analysis. In the CD8 + subgroup, due to a technical issue during sample processing, LC–MS/MS analysis could not be performed on one set of samples. Therefore, the CD8 + group analysis was conducted with 17 AD and 17 control samples (AD: Age = 74.4 ± 4.4, M/F = 9/8, CDR = 1.6 ± 0.6, MMSE = 18.1 ± 3.4; Control: Age = 67.5 ± 7.8, M/F = 8/9).

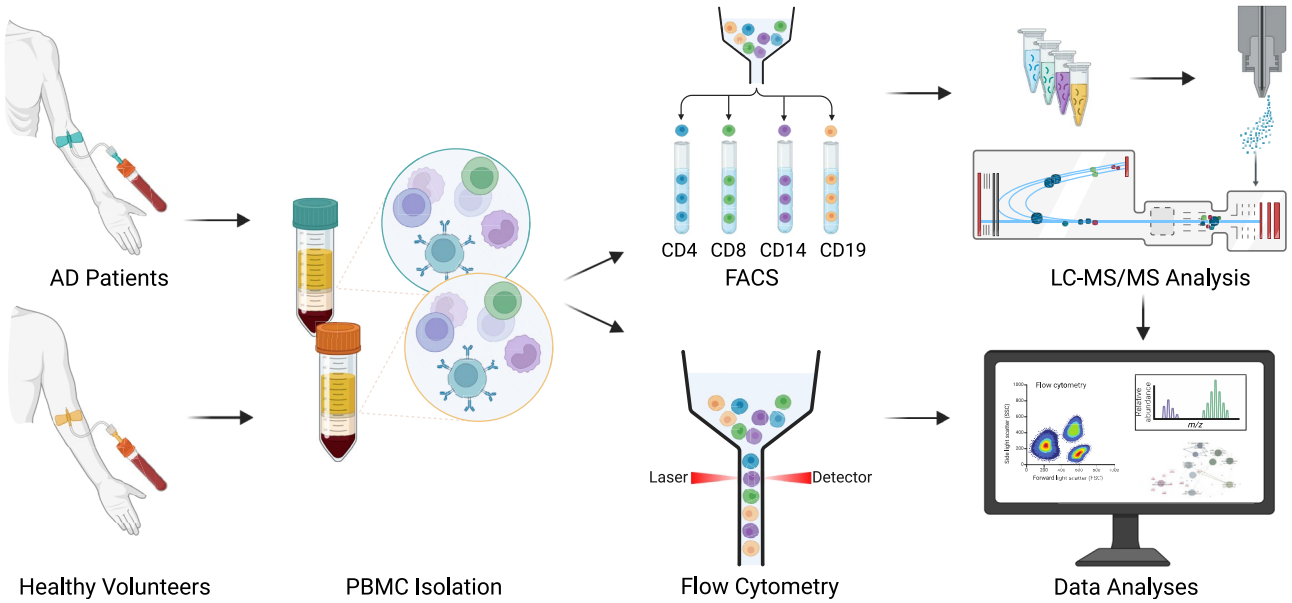

Fig. 1. Study design overview. PBMCs were isolated from blood samples collected AD patients and age-matched healthy controls. The isolated PBMCs were then subjected FACS to separate them into four distinct cell subpopulations: CD4 +, CD8 +, CD14 +, and CD19 +. The proteomic profiles of the sorted cell subpopulations were analyzed using LC–MS/MS. Also isolated PBMC was stained with antibodies specific to the four cell subpopulations, followed by flow cytometry-based mitochondrial functional assays. Lastly, the analysis of the data obtained from LC–MS/MS and flow cytometry analyses was conducted. Created in BioRender. Kiris, I. (2025) https://BioRender.com/s70y444.

	Control	AD
Total	23	20
Male/Female	15/8	10/10
Age	66.1 ± 7.2	74.3 ± 4.7
CDR	/	1.9 ± 0.6
MMSE	/	16.9 ± 3.1

Table 1. Demographic and clinical characteristics of AD and control.

PBMC isolation

PBMCs were isolated from freshly drawn whole blood using density gradient centrifugation (Ficoll Paque PLUS; GE Healthcare) in a Sepmate PBMC isolation tubes (STEMCELL Technologies, Vancouver, Canada) following the manufacturer's instructions. In short, Ficoll Paque gradient was placed to the bottom of tubes and the diluted blood at a ratio of 1:1 with Dulbecco's phosphate-buffered saline (DPBS) carefully layered over tubes. The tubes were centrifuged at 2000 rpm for 25 min. The cell interface layer was carefully collected, and the cells were washed in RPMI by centrifugation at 1400 rpm for 10 min. After counting, the cell suspension was aliquoted into cryovials with freezing media and stored at −80°C until further use.

Fluorescence-activated cell sorting (FACS)

Fluorescence-activated cell sorting (FACS) was performed with PBMC samples of AD patients and controls to isolate CD4 +, CD8 +, CD14 + and, CD19 + cell populations using the MA900 Multi-Application Cell Sorter (Sony Biotechnology). Frozen aliquots of PBMCs were washed, counted, and suspended in RPMI at 37°C. PBMCs were then incubated for 30 min with the following antibodies: CD3 (BV605;Biolegend;Cat#317,322), CD14 (A700;Biolegend;Cat#325,614), CD19 (PeCy7;Biolegend;Cat#302,216), CD4 (BV510;Biolegend;Cat#317,444), CD8 (Pacific Blue;Biolegend;Cat#301,033) for 30 min. The stained cells were sorted by MA900 Multi-Application Cell Sorter (Sony Biotechnology).

Live cells were defined by a forward and side scatter gate and then separated by CD3 + and CD14 +. CD3 + cells were further sub-gated into specific T cell populations (CD4 + and CD8 +). Also, B lymphocytes separated by CD19 +. As a result of sorting, four (CD4 +, CD8 +, CD14 +, CD19 +) cell subgroups were obtained. The obtained sorted cells were counted and frozen with liquid nitrogen.

Sample preparation for LC–MS/MS analysis

Sample preparation was performed as previously reported[24] with an extra step of acetone precipitation. Briefly, the FACS sorted cell pellets were lysed in Universal Protein Extraction kit (UPX, Expedeon) with protease inhibitor cocktail (Thermo Scientific) and homogenized. Then four volumes of ice-cold acetone were added to each sample and incubated at −20°C for an hour. Following a centrifugation at 18,000 g at + 4°C for 5 min, acetone was removed and the pellet was air-dried for 1 min. After another round of dissolving and homogenization, samples were processed with filter-aided sample preparation method to obtain tryptic peptides.

LC–MS/MS parameters

ACQUITY UPLC M-Class coupled SYNAPT Xevo G2-XS system (Waters) was used for protein expression analysis. The analysis was conducted as previously reported[24]. Briefly, the column was preheated to 45°C and equilibrated with 97% mobile phase A. Concisely, tryptic peptides were loaded onto a trap column, and then separated using a gradient elution method. As a lock mass reference, Glu-1-fibrinopeptide B (Glu-fib) was used. Positive ion mode was used to operate the MS instrument. The quadrupole was continuously scanned between m/z 400 to 900 in data independent acquisation mode SONAR, with a transmission width of 24 Da. Sequential MS and MS/MS scans were carried out at 10 V and 40 V for low and high collision energy, respectively. In the sensitivity mode, all ions between 50-1950 m/z were fragmented together without any precursor ion preselection. The retention time of fragmented ion data was used to align it with the corresponding precursors.

LC–MS/MS data processing

For the quantitative analysis of peptide features and protein identification, the Progenesis-QI for proteomics software (V.2.0 Waters) was used. The calibrant was Glu-fib peptide with m/z 785.8426, and the sample sets were normalized based on total ion intensity. For high and low energy thresholds, processing parameters were set 60 to 10 respectively. All mass data were imported into Progenesis QI and analyzed using the following parameters: minimum number of fragmented ion matches per peptide = 2, a minimum number of fragmented ion matches per protein = 5, a minimum number of unique peptides per protein = 1, the maximum number of missed cleavages for tryptic digestion = 1. The fixed modification is carbamidomethyl C, the variable modifications are oxidation M and deamidation N and Q, and the false discovery rate (FDR) is less than 1%. Only 2 + and 3 + ion charges were chosen. Protein normalization was performed according to the relative quantitation using non-conflicting peptides, expressional changes along with p and q values were calculated using the statistical package included in Progenesis QI for proteomics. The resulting data set was filtered by following criteria: ANOVA p value ≤ 0.05, q value ≤ 0.05, at least 2 unique peptides per protein, and a minimum of 1.5-fold change in expression between AD and control groups within each cell type.

Principal Component Analysis (PCA) was performed for both CD4 + and CD8 + T cell groups using ClustVis (https://biit.cs.ut.ee/clustvis/) (Fig. 2). The significance and expression changes of identified proteins are presented using a volcano plot generated with the ggplot2 R package[25] (Fig. 2).

Gene ontology and pathway enrichment analysis

Gene ontology analysis (GO) serves as a valuable tool for functionally annotating differentially expressed proteins (DEPs) within a biological context, particularly in relation to biological processes (BP), cellular components (CC), and molecular functions (MF)[26]. To elucidate the functional roles of these proteins and establish connections with molecular pathways, the Kyoto Encyclopedia of Genes and Genomes (KEGG; http://www.kegg.jp/) pathway database was used[27]. GO term and KEGG pathway enrichment analyses for DEPs were conducted using the Database for Annotation, Visualization, and Integrated Discovery (DAVID) online resource (DAVID Bioinformatics Resources 2021). An adjusted p value (Benjamini correction) of < 0.05 was established as the cutoff criterion, and the data was sorted by ratio. Additionally, "ggplot2" and "GOplot" R packages were used to visualize the most significant GO terms and KEGG pathways and their associated proteins[25,28]. To complement standard enrichment analyses, Gene Set Enrichment Analysis (GSEA) was conducted using a pre-ranked list of all quantified proteins based on fold-change values between AD and control for each cell type. Analyses were performed using GSEA desktop tool (version 4.4.0, Broad Institute) with KEGG[29] and GO gene sets. Nominal p-values < 0.05 were considered significant. GSEA results are provided in Supplementary Figs. 1–5.

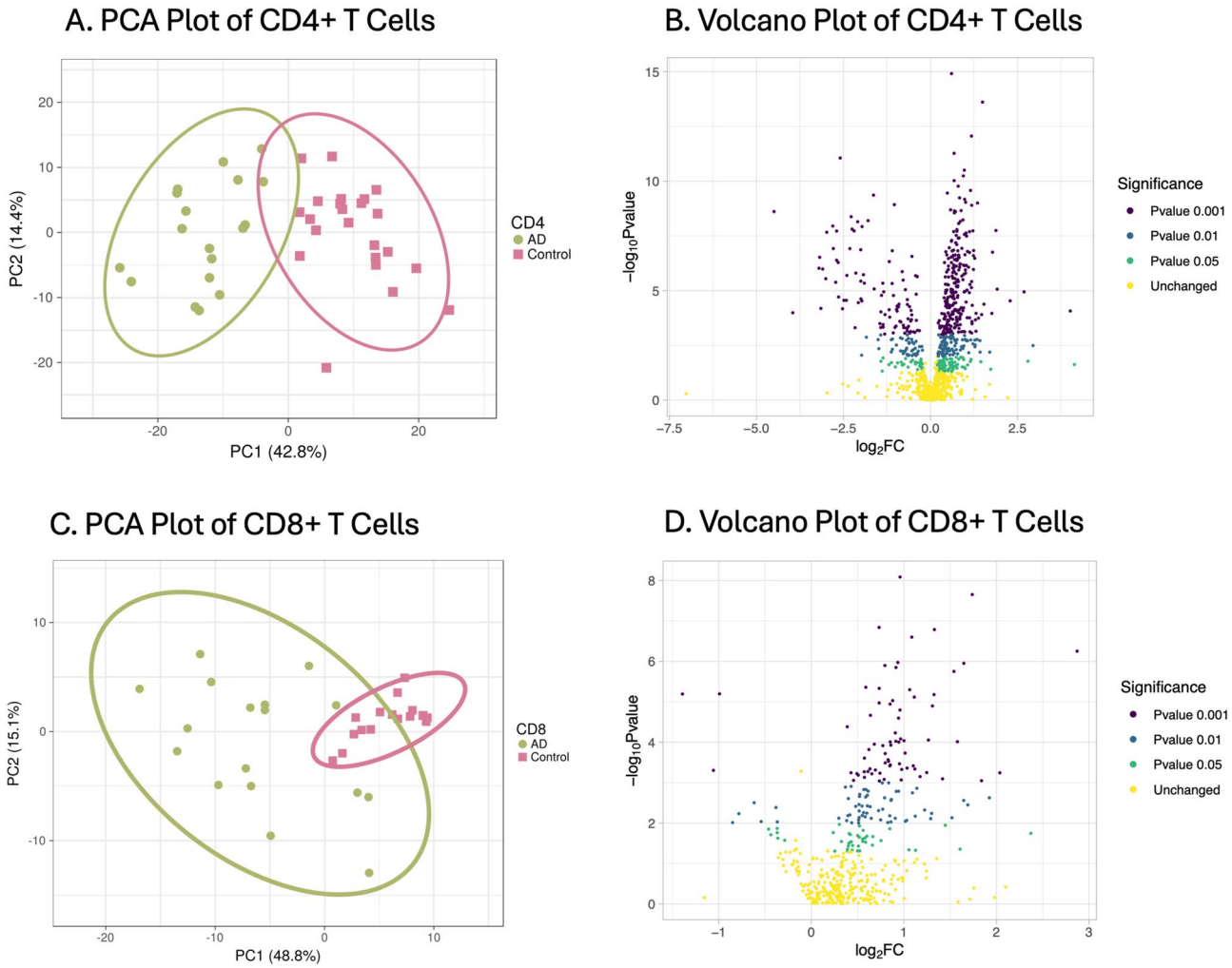

Fig. 2. PCA and volcano plot analysis of CD4 + and CD8 + T cells proteomes in AD and control. (**A**) PCA plot of CD4 + T cells based on DEPs. (**B**) Volcano plots showing identified proteins in CD4 + T cells. (**C**) PCA plot of CD8 + T cells based on DEPs. (**D**) Volcano plot showing identified proteins in CD8 + T cells. In volcano plots, the x-axis shows the $\log_2$ fold change ($\log_2$FC) comparing AD to controls. The y-axis represents the $-\log_{10}$ p value. Colored dots indicate significantly altered proteins (p value < 0.001, < 0.01, < 0.05), while yellow dots show proteins with no significant change.

Protein–protein interaction and hub proteins identification

The protein–protein interaction (PPI) network for DEPs of CD4 + and CD8 + was established using STRING database protein query[30]. A statistical significance threshold was defined, requiring a combined score exceeding 0.4. Subsequently, the PPI network was visualized using Cytoscape[31] (version 3.9.1.). The "cytohubba" Cytoscape plugin[32] was then used to score the genes based on their network features in order to identify hub proteins in the PPI network. Maximum neighborhood component (MNC), maximal clique centrality (MCC), edge percolated component (EPC) results were used to select hub proteins in this study. The "Omics Visualizer" Cytoscape plugin[33] was used to visualize the hub proteins network and expression level. To comprehensively analyze the functional characterization of hub proteins and explore the relationships between these functional terms, we utilized the ClueGO plugin within Cytoscape[34]. This plugin constructs a "functional annotation network," where similar functional terms are grouped together and reveals how these terms are interconnected. In the ClueGO analysis, GO Enrichment (BP) and KEGG Pathway terms were examined, and the p-value was adjusted by the Benjamini–Hochberg method with a significance threshold set at $p \leq 0.01$.

Mitochondrial superoxide measurement

We used the live PBMC cells that we had previously frozen for the Flow Cytometry assays. Superoxide levels were measured following the incubation of isolated PBMC with the antibodies similar to FACS analysis. Mitochondrial superoxide production was assessed using Mitosox Red (Thermo Fisher Scientific, Cat. No. M36008, Waltham, MA), a fluorogenic dye detects mitochondrial superoxide in live cells. Cells were incubated with 4 µM Mitosox Red for 15 min and measured using flow cytometer Cytek Aurora (Cytek Biosciences). To ensure consistency across samples, each experiment was initiated with 1 million PBMCs per sample, and the same number of gated events was collected during flow cytometry acquisition. Flow cytometry data results were then processed and analyzed using FlowJo software (v10, BD Life Sciences).

Mitochondrial membrane potential (ΔΨm) analysis

Similar to the procedure described in superoxide measurement, PBMCs were incubated with antibodies before conducting the analysis of ΔΨm. The mitochondrial membrane potential was assessed using JC-1 (Thermo Fisher Scientific, No. T3168, Waltham, MA). Cells were incubated with 0.3 µg/ml JC-1 for 10 min. Mitochondrial depolarization was identified by an decrease in red fluorescence (aggregate form, absorption/emission at 585/590 nm) and a increase in green fluorescence (monomeric form, absorption/emission at 510/527 nm)[35]. To further evaluate mitochondrial function, valinomycin (Thermo Fisher Scientific,V1644 Waltham, MA) was used to disrupt the mitochondrial electrochemical gradient by facilitating K^+ ion transport across the mitochondrial membrane[36]. Subsequently, the cells were analyzed using the Cytek Aurora flow cytometer**.** The results obtained from flow cytometry data were then processed and analyzed using FlowJo software. Experiments were performed using the same initial PBMC count and gating strategy as described above.

Statistical analysis

Graphpad Prism software (version 10.2.3 GraphPad Software, La Jolla California USA, www.graphpad.com) was used for statistical analysis of JC-1 and Mitosox Red assays. Results were compared both across different cell subsets and within each cell group. Statistical differences between two groups were assessed using the t-test or the Mann–Whitney U test, depending on data distribution. Comparisons among three or more groups were performed using one-way ANOVA with Dunnett's post hoc test or Kruskal–Wallis test followed by Dunn's multiple comparison. For multiple comparisons involving two independent variables, two-way ANOVA with Tukey's post-hoc test was used. Data was shown as mean +/- standard deviation (SD). Statistical significance was defined as *$p < 0.05$ (* or #), $p < 0.01$ (**), $p < 0.001$(***), $p < 0.0001$ (****).*

Results

Proteomic analysis of CD4 + subgroup: significantly altered proteins and pathways

The LC–MS/MS analysis identified a total of 1,352 proteins within the CD4 + subgroup, of which 387 proteins displayed significant differential expression in the AD group compared to the control group (fold change ≥ 1.5; unique peptide ≥ 2; q value ≤ 0.05 and p value ≤ 0.05). The significance and expression levels of the identified proteins are detailed in the volcano plot in Fig. 2B.

To conduct functional enrichment and PPI analyses, we utilized 387 DEPS in the CD4 + subgroup. PCA revealed that the proteome of 18 AD patients and 23 age-matched control group were distinctly separated along PC1 (42.8%) and PC2 (14.4%), as shown in Fig. 2A.

GO and KEGG enrichment analyses were conducted using the DAVID online tool. GO enrichment analysis revealed that the DEPs were most significantly enriched in BP terms related to nucleosome assembly, cytoplasmic translation, and translation (Fig. 3A). The MF terms were protein binding, RNA binding and identical protein binding (Fig. 3B). Additionally the CC terms included the cytosol, extracellular exosome, and nucleus (Fig. 3C). The top enriched GO terms and relevant genes were visualized in a chord graph (Fig. 3D). The KEGG pathways analysis indicated that proteins were related to neutrophil extracellular trap formation, pathways of neurodegeneration-multiple diseases, Amyotrophic lateral sclerosis (ALS), Parkinson disease (PD), Prion disease (PrD), Huntington disease (HD), AD and ribosome (Fig. 3E). Gene Set Enrichment Analysis (GSEA) was also performed using the full ranked proteomic dataset for CD4 + T cells. GSEA identified similar enrichment patterns, including neurodegeneration-related pathways (e.g., AD, Huntington's disease) and key metabolic processes such as the citrate cycle (TCA), aerobic respiration, and cellular respiration (Supplementary Fig. 1–2). These results support the robustness of our enrichment analysis and further highlight the relevance of mitochondrial and metabolic alterations in CD4 + T cells in AD. Additionally, twelve hub proteins identified in the CD4 + T cell analysis —CCT8, EEF2, EIF5A, HNRNPA1, HNRNPK, RPL8, RPL15, RPLP2, RPS6, RPS14,

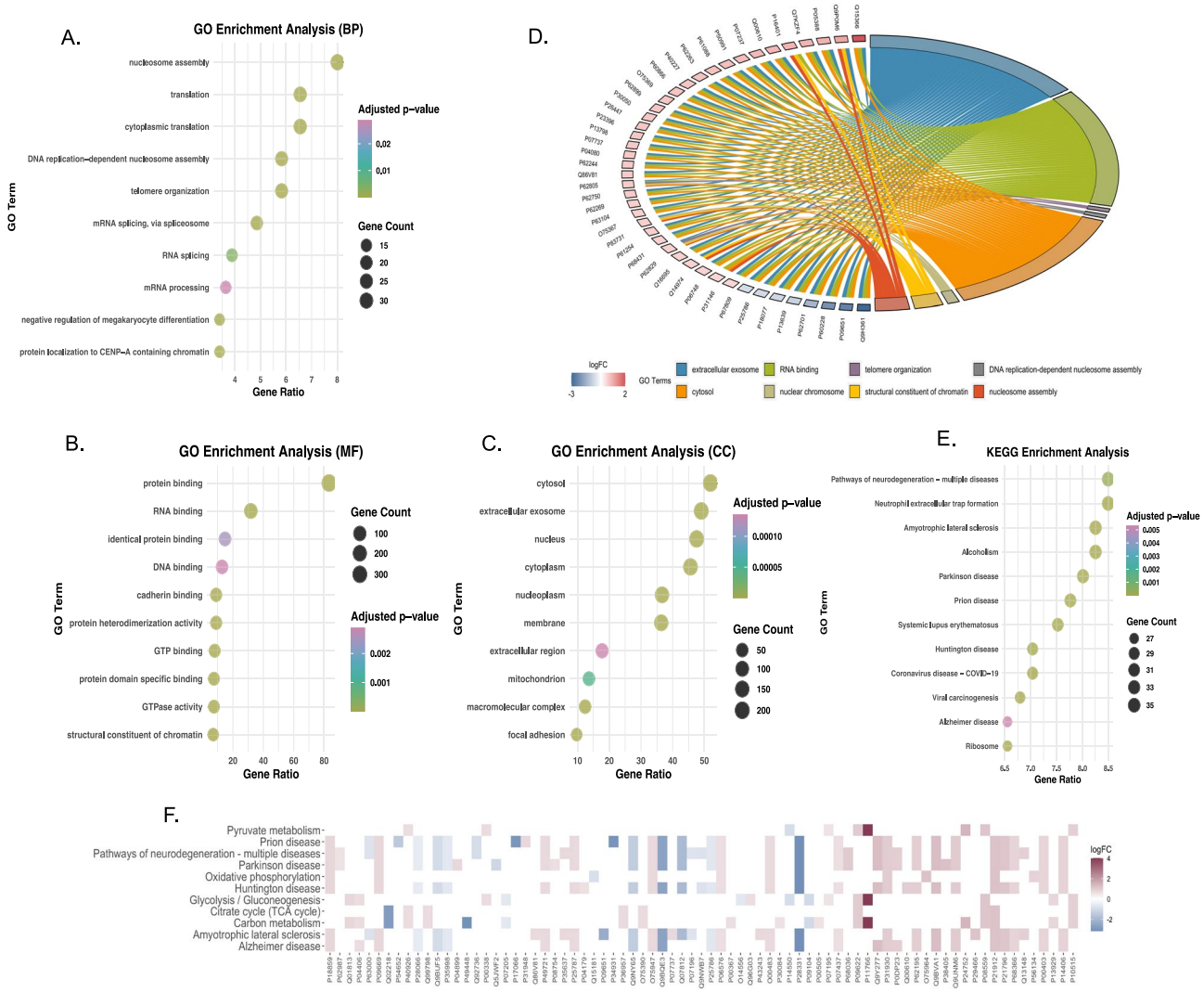

Fig. 3. Functional enrichment analysis of DEPs in CD4 + T cells. (**A**-**B**-**C**) The graphs represent enriched GO (MF: Molecular function, BP: Biological process, CC: Cellular component) terms for DEPs in CD4 + T cells. (**D**) Chord diagram of the most significant enriched GO terms for DEPs in CD4 + T cells. UniProt names and their corresponding fold changes are shown on the left, while colored lines indicate the association of proteins with different GO terms. (**E**) Bubble chart showing enriched KEGG terms for DEPs in CD4 + T cells. (**F**) Heatmap of proteins involving in neurodegeneration and energy metabolism associated GO and KEGG terms.

RPS15A, and SRSF1—were also present among the top-ranked proteins visualized in the GSEA heatmap, further supporting their relevance to the observed pathway enrichments (Supplementary Fig. 3).

In order to elucidate the relationship between AD and energy metabolism in CD4 + cells, expression of the proteins were investigated that are enriched in relevant GO and KEGG terms. These terms included pathways related to neurodegenerative disorders such as neurodegeneration-multiple diseases, ALS, PD, PrD, HD, AD, as well as metabolic pathways including carbon metabolism, glycolysis/gluconeogenesis, citrate cycle (TCA), pyruvate metabolism, and oxidative phosphorylation. The results indicated that 76 proteins were related to both AD and energy metabolism (Fig. 3F).

PPI Network of CD4 + subgroup with DEPs and identification of hub proteins

The PPI network for 387 DEPS in the CD4 + subgroup was constructed using STRING database protein query. Cytoscape was employed to visualize the PPI network, which consisted of 379 nodes and 4203 edges.

The cytoHubba plugin of Cytoscape software was utilized to identify proteins with higher degrees, indicating the most significant roles and connections within the network. The top 20 hub proteins calculated by MNC, MCC and EPC algorithms (Fig. 4A-C). The intersection of hub proteins across all three algorithms consisted of EEF2, RPL26, RPL9, RPS20, RPS3, RPLP0, RPL12, RPS14, and RPL8 (Fig. 4D). The total number of hub proteins obtained is 32 and are as follows: RPL17, RPS18, RPL23A, RPS15A, RPL35A, RPL23, ATP5B, SNRPD3, SNRPF, HNRNPK, SRSF1, RPLP2, EIF5A, RPS23, RPS7, RPL15, RPS4X, CCT4, CCT8, EIF4A3, GAPDH, HNRNPA1,

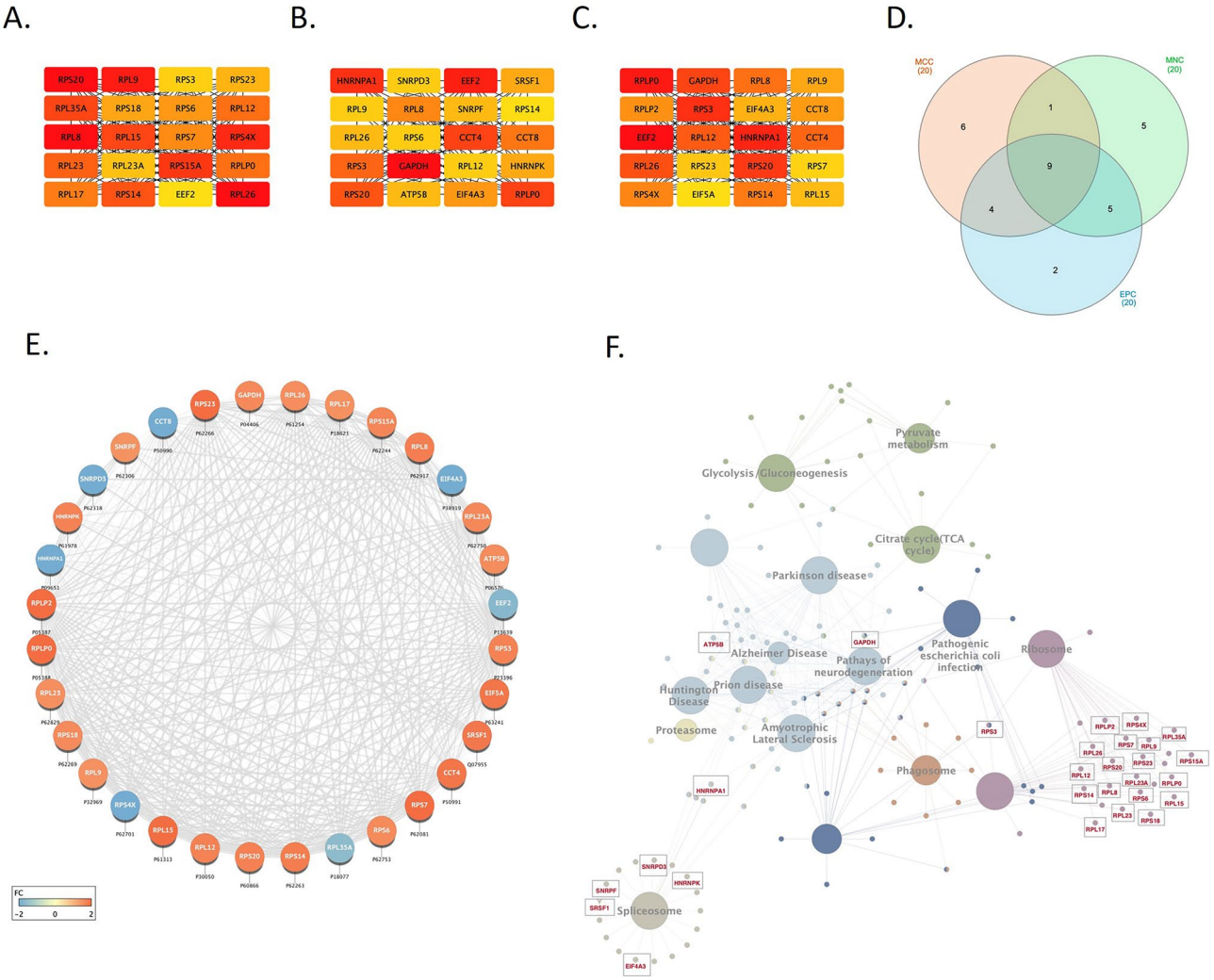

Fig. 4. Hub protein analysis of CD4 + T cells. (**A**,**B**,**C**) The cytoHubba plugin in Cytoscape was used to identify the top 20 hub proteins by MNC, MCC, and EPC algorithms. (**D**) Venn diagram showing the common hub proteins identified by the EPC, MCC, and MNC algorithms. (**E**) The interaction network and the expression levels CD4 + T cell hub proteins. (**F**) KEGG pathway enrichment analysis of DEPs in CD4 + T cells, highlighting the pathways in which hub proteins are significantly involved.

EEF2, RPL26, RPL9, RPS20, RPS3, RPLP0, RPL12, RPS14, RPL8, RPS6 are listed with brief descriptions in Table 2.

The network and expression levels of these proteins are shown in Fig. 4E. The results indicate that these proteins are highly interconnected, with 25 proteins exhibiting upregulated expression, and 7 proteins showing downregulated expression relative to the control group.

The results of ClueGO analysis, which shows the association of these hub proteins with pathways significantly altered in the CD4 + T cell are presented in Fig. 4F. The hub proteins ATP5B, HNRPA1, and GAPDH are implicated in pathways related to neurodegenerative disorders, including ALS, PD, PrD, HD, and AD. Moreover, GAPDH is also involved in processes such as glycolysis/ggenesis, TCA, pyruvate metabolism, and the pathogenic Escherichia coli (*E.coli*) infection pathway. Additionally, EIF4A3, HNRNPK, HNRNPA1, SNRPD3, SRSF1, and SNRPF play vital roles within the spliceosome complex. Furthermore, several other ribosomal hub proteins are associated with the ribosome pathway.

Proteomic analysis of CD8 + subgroup: significantly altered proteins and pathways

The LC–MS/MS analysis results identified 569 proteins within the CD8 + subgroup, among which 121 proteins exhibited a significant difference in expression between AD and the control group fold change ≥ 1.5; unique peptide ≥ 2; $q \leq 0.05$, and $p \leq 0.05$). The significance and expression levels of the identified proteins are detailed in the volcano plot in Fig. 2D.

To conduct functional enrichment and PPI analysis, we utilized 121 DEPs in the CD8 + subgroup. The proteomes of 17 AD patients and 17 age-matched control group were differentiated along PC1 (48.8%) and PC2 (15.1%), as shown in Fig. 2C.

Uniprot ID	Name	Description	Fold change	DIFF_State
P18621	RPL17	60S ribosomal protein L17	1.5	Up
P62269	RPS18	40S ribosomal protein S18	1.6	Up
P62750	RPL23A	60S ribosomal protein L23a	1.6	Up
P62244	RPS15A	Small ribosomal subunit protein uS8	1.6	Up
P18077	RPL35A	60S ribosomal protein L35a	1.6	Down
P62829	RPL23	60S ribosomal protein L23	1.5	Up
P06576	ATP5B	ATP synthase subunit beta_ mitochondrial	1.6	Up
P62318	SNRPD3	Small nuclear ribonucleoprotein Sm D3	3.6	Down
P62306	SNRPF	Small nuclear ribonucleoprotein F	1.5	Up
P61978	HNRNPK	Heterogeneous nuclear ribonucleoprotein K	1.7	Up
Q07955	SRSF1	Serine/arginine-rich splicing factor 1	1.8	Up
P05387	RPLP2	Large ribosomal subunit protein P2	2.4	Up
P63241	EIF5A	Eukaryotic translation initiation factor 5A-1	1.9	Up
P62266	RPS23	Small ribosomal subunit protein uS12	2.1	Up
P62081	RPS7	Small ribosomal subunit protein eS7	2.1	Up
P61313	RPL15	Large ribosomal subunit protein eL15	1.9	Up
P62701	RPS4X	Small ribosomal subunit protein eS4, X isoform	2.5	Down
P50991	CCT4	T-complex protein 1 subunit delta	1.8	Up
P50990	CCT8	T-complex protein 1 subunit theta	4.6	Down
P38919	EIF4A3	Eukaryotic initiation factor 4A-III	2.7	Down
P04406	GAPDH	Glyceraldehyde-3-phosphate dehydrogenase	1.6	Up
P09651	HNRNPA1	Heterogeneous nuclear ribonucleoprotein A1	4.9	Down
P13639	EEF2	Elongation factor 2	1.7	Down
P61254	RPL26	Large ribosomal subunit protein uL24	1.5	Up
P32969	RPL9	Large ribosomal subunit protein uL6	1.5	Up
P60866	RPS20	Small ribosomal subunit protein uS10	1.7	Up
P23396	RPS3	Small ribosomal subunit protein uS3	1.7	Up
P05388	RPLP0	Large ribosomal subunit protein uL10	2.0	Up
P30050	RPL12	Large ribosomal subunit protein uL11	1.7	Up
P62263	RPS14	Small ribosomal subunit protein uS11	1.7	Up
P62917	RPL8	Large ribosomal subunit protein uL2	1.7	Up
P62753	RPS6	Small ribosomal subunit protein eS6	1.5	Up

Table 2. Hub proteins list of CD4 + T cell.

GO enrichment analysis revealed that the DEPs were most significantly enriched in BP terms associated with negative regulation of the apoptotic process, protein folding, and protein refolding (as shown in Fig. 5A), in the MF terms related with protein binding, RNA binding, and cadherin binding (Fig. 5B) and CC terms included extracellular exosome, cytosol, and cytoplasm (Fig. 5C). The top enriched GO terms and their associated genes were visually represented in a chord graph (Fig. 5D). KEGG enrichment analysis identified terms associated with pathogenic E.coli infection, endocytosis, tight junctions, regulation of the actin cytoskeleton, carbon metabolism, and glycolysis/gluconeogenesis (Fig. 5E). To complement these findings, Gene Set Enrichment Analysis (GSEA) was performed on the full ranked proteomic dataset for CD8 + T cells. While the overall number of quantified proteins was limited compared to CD4 + cells, GSEA still revealed consistent enrichment of pathways such as positive regulation of protein catabolic processes, spliceosome, cell junction organization, and guanyl nucleotide binding, further supporting the involvement of protein turnover, RNA metabolism, and cytoskeletal remodeling in AD-associated CD8 + T cell dysfunction (Supplementary Fig. 4). Additionally, eleven hub proteins identified in the CD8 + T cell analysis — ENO2, GLUD1, HSP90AA1, HSPA8, HSPD1, LDHC, PGK1, PKM, RHOA, RPSA, TKT — were also present among the top-ranked proteins visualized in the GSEA heatmap, further supporting their relevance to the observed pathway enrichments (Supplementary Fig. 5).

Proteins and their corresponding expression levels that are associated with GO and KEGG terms related to neurodegeneration and energy metabolism in the CD8 + cell group were presented in Fig. 5F. The terms include unfolded protein binding, RNA binding, response to unfolded protein, protein refolding, oxygen transporter activity, hydrogen peroxidase catabolic process, GTPase activity, glycolysis/gluconeogenesis, carbon metabolism, and cadherin binding. These terms are associated with 61 proteins that have been significantly altered in the CD8 + cell group.

PPI network of CD8 + subgroup with DEPs and identification of hub proteins

STRING was utilized to construct the PPI network for the CD8 + subgroup, comprising 121 DEPs. The network, consisting of 119 nodes and 488 edges, was visualized using Cytoscape software.

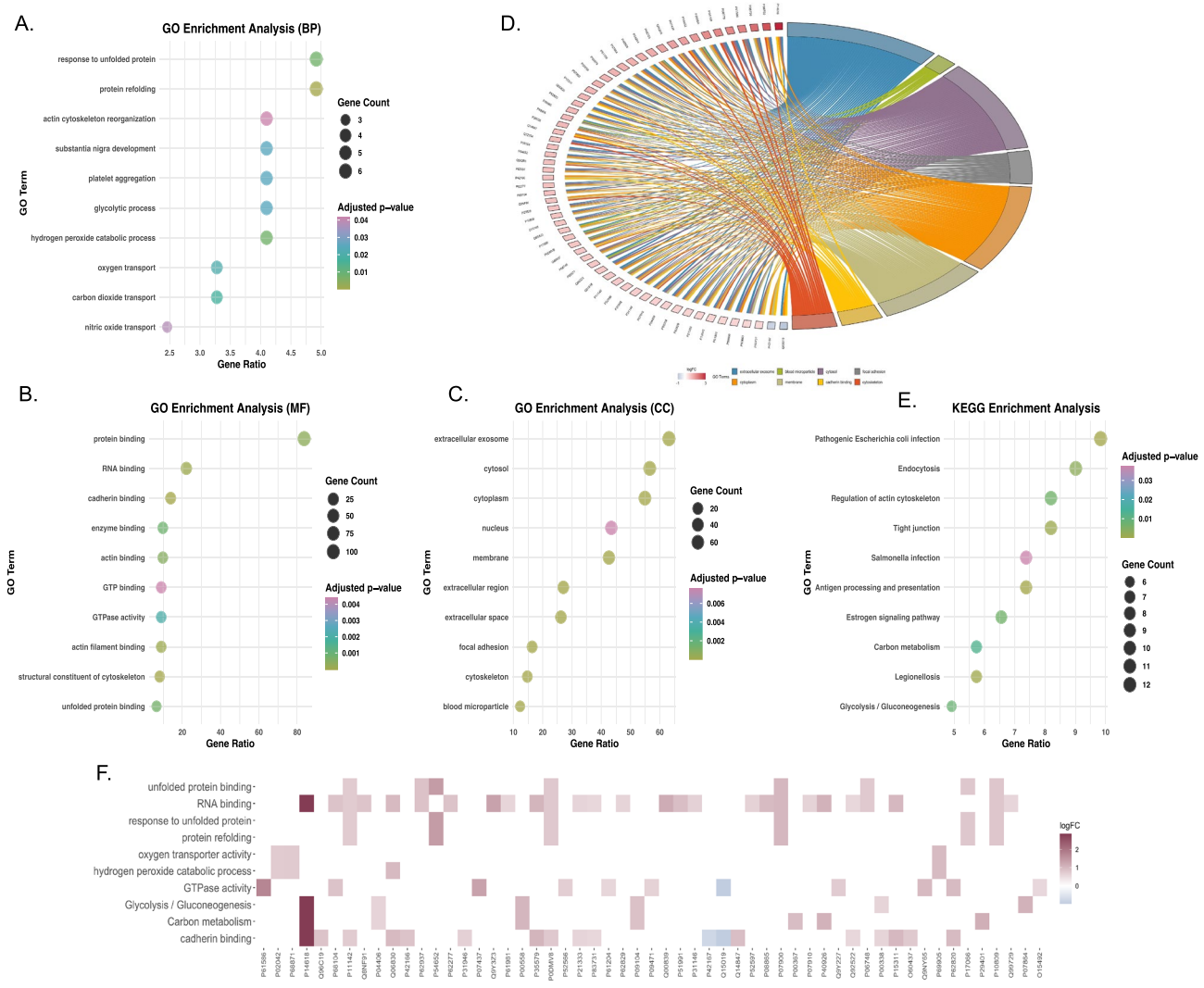

Fig. 5. Functional enrichment analysis of DEPs in CD8 + T cells. (**A**-**B**-**C**) The graphs represent enriched GO (MF: Molecular function, BP: Biological process, CC: Cellular component) terms for DEPs in CD8 + T cells. (**D**) Chord diagram of the most significant enriched GO terms for DEPs in CD8 + T cells. UniProt names and their corresponding fold changes are shown on the left, while colored lines indicate the association of proteins with different GO terms. (**E**) Bubble chart showing enriched KEGG terms for DEPs in CD8 + T cells (**F**) Heatmap of proteins involving in neurodegeneration and energy metabolism associated GO and KEGG terms.

In the CD8 + subgroup, similar to the hub analysis conducted in the CD4 + subgroup, the cytoHubba plug-in of the Cytoscape software was employed.

Using MNC, MCC, and EPC algorithms, the top 10 hub proteins were identified, with HSPA8, PKM, GAPDH, and LDHA notably identified as common hub proteins across all three algorithms (Fig. 6A-D). The total 17 hub proteins was identified, and presented in Table 3, along with concise descriptions. These hub proteins include CFL1, EEF1A1, ENO2, GAPDH, GLUD1, HSP90AA1, HSPA8, HSPD1, LDHA, LDHC, MDH2, MYH9, PGK1, PKM, RHOA, RPSA, and TKT.

Figure 6E displays the connections and expression levels of these hub proteins. It is noteworthy that all the hub proteins exhibit high interconnectivity and demonstrate upregulated expression in the AD group.

To assess the significance of hub proteins in the pathways and processes involving DEPs the CD8 + group, we conducted a ClueGO analysis, similar to the one performed in the CD4 + group (Fig. 6F). The hub proteins EEF1A1, HSP90AA1, HSPA8, and HSPD1 are implicated in processes related to protein folding, encompassing roles as protein folding chaperones, 'de novo' protein folding, protein refolding, ATP-dependent protein folding chaperones, and also involvement in antigen processing and presentation. The hub proteins MYH9, CFL1, and RHOA play a role in Pathogenic E.coli infection and the regulation of actin cytoskeleton. MYH9 is also associated with the process of structural constituent of cytoskeleton. Additionally, ENO2, GAPDH, LDHA, LDHC, PGK1, and PKM are linked to the pathways of glycolysis/gluconeogenesis.

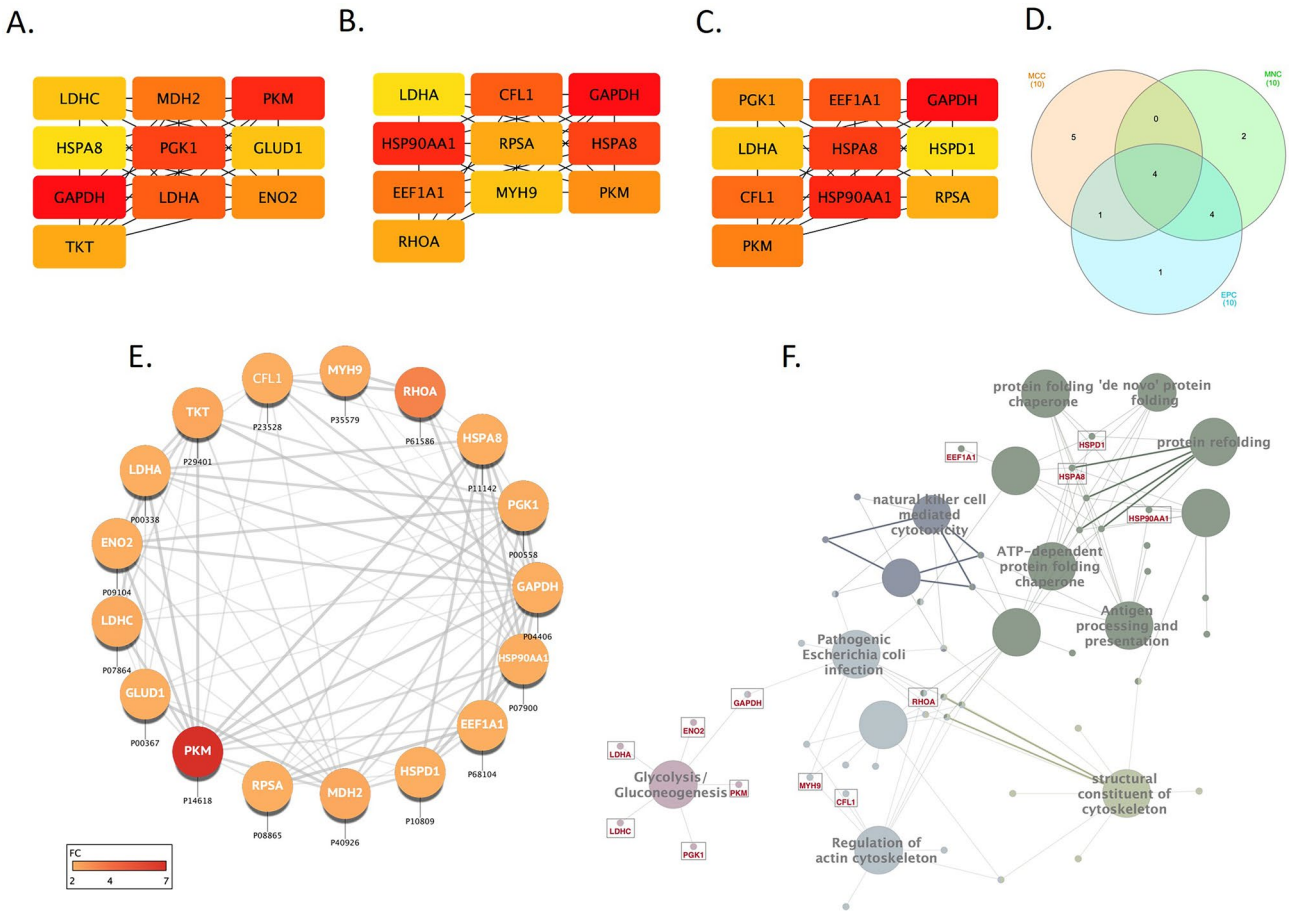

Fig. 6. Hub protein analysis of CD8 + T cells.(**A**,**B**,**C**) The cytoHubba plugin in Cytoscape was used to identify the top 10 hub proteins by MNC, MCC, and EPC algorithms. (**D**) Venn diagram showing the common hub proteins identified by the EPC, MCC, and MNC algorithms. (**E**) The interaction network and the expression levels CD8 + T cell hub proteins. (**F**) KEGG pathways and biological processes terms of DEPs in CD8 + T cells, highlighting the terms in which hub proteins are significantly involved.

Uniprot ID	Gene name	Description	Fold change	DIFF-State
P00367	GLUD1	Glutamate dehydrogenase 1, mitochondrial	1.9	Up
P07864	LDHC	L-lactate dehydrogenase C chain	2.1	Up
P29401	TKT	Transketolase	2.2	Up
P09104	ENO2	Gamma-enolase	1.8	Up
P40926	MDH2	Malate dehydrogenase, mitochondrial	2.1	Up
P61586	RHOA	Transforming protein RhoA	3.3	Up
P35579	MYH9	Myosin-9	2.0	Up
P10809	HSPD1	60 kDa heat shock protein, mitochondrial	1.7	Up
P00558	PGK1	Phosphoglycerate kinase 1	2.0	Up
P68104	EEF1A1	Elongation factor 1-alpha 1	1.7	Up
P07900	HSP90AA1	Heat shock protein HSP 90-alpha	2.0	Up
P23528	CFL1	Cofilin-1	1.7	Up
P08865	RPSA	Small ribosomal subunit protein uS2	1.9	Up
P11142	HSPA8	Heat shock cognate 71 kDa protein	1.6	Up
P14618	PKM	Pyruvate kinase PKM	7.3	Up
P04406	GAPDH	Glyceraldehyde-3-phosphate dehydrogenase	1.5	Up
P00338	LDHA	L-lactate dehydrogenase A chain	1.5	Up

Table 3. List of hub proteins identified in CD8 + T cell.

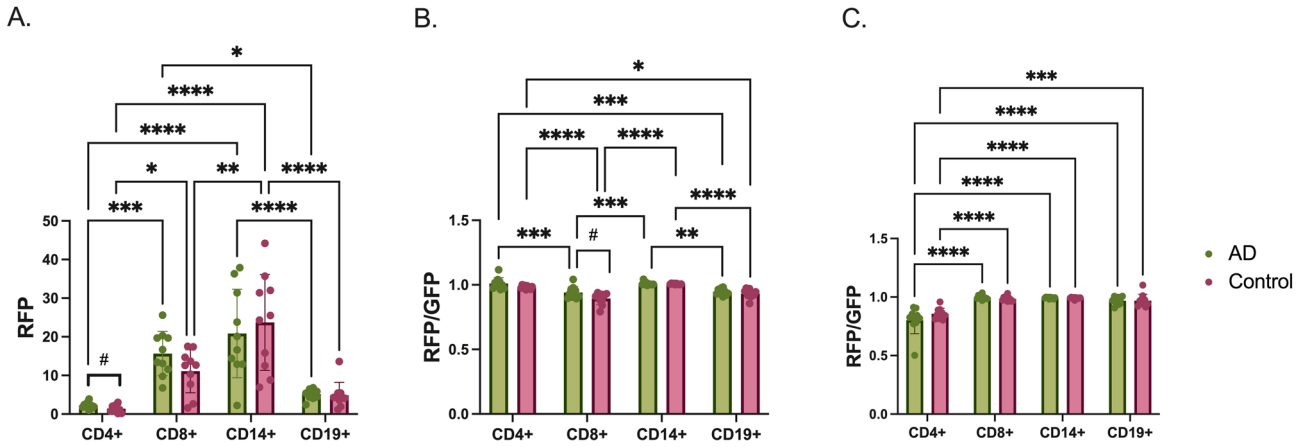

Fig. 7. Mitochondrial ROS levels and ΔΨm in CD4 +, CD8 +, CD14 +, and CD19 + cell subsets were analyzed through multiple comparisons across cell subsets and within each cell group. (**A**) ROS levels indicated by RFP. (**B**) JC-1 assay results based on the red/green ratio. (**C**) JC-1 results of valinomycin-induced cells. Data were analyzed using two-way ANOVA with Tukey's post hoc multiple comparison test and unpaired t-test for comparision of whithin each cell group. Graphs are presented as mean ± SD. $p < 0.05$ (* or #), $p \leq 0.01$ (**), $p \leq 0.001$(***), $p \leq 0.0001$.

Mitochondrial ROS alterations in AD: A comparative analysis of CD4 +, CD8 +, CD14 +, and CD19 + subgroups

The levels of mitochondrial ROS in CD4 +, CD8 +, CD14 +, and CD19 + cell subsets, assessed using MitoSOX Red, were quantified in 10 AD patients and 10 controls. These levels, represented by RFP fluorescence intensity, are presented in Fig. 7A. A two-way ANOVA and unpaired t-test was performed to evaluate the differences in mitochondrial ROS levels among the cell subsets (CD4 +, CD8 +, CD14 +, and CD19 +) in AD and control groups, as well as their interaction. Mitochondrial ROS levels showed notable differences between cell subsets and between AD and control groups. In the AD group, CD4 + cells had significantly lower ROS levels compared to CD8 + ($p = 0.0008$) and CD14 + cells ($p < 0.0001$). Additionally, CD14 + cells in the AD group exhibited significantly higher ROS levels compared to other cell types in the control group ($p < 0.0001$). Interestingly, when comparing AD and control groups within each cell subset, only CD4 + cells showed significantly higher ROS levels in AD patients compared to controls ($p < 0.05$), while no significant differences were observed in other subsets (Supplementary Fig. 6B-E). Importantly, when ROS levels were compared independently of cell type, no significant difference was found between AD and control groups (Supplementary Fig. 6A), highlighting the cell-type-specific nature of oxidative stress alterations in AD.

Differential mitochondrial membrane potential and valinomycin response in CD4 +, CD8 +, CD14 +, and CD19 + Cells in AD

The JC-1 assay was used to evaluate ΔΨm in four cell subgroups by measuring the red/green fluorescence ratio, which reflects changes in mitochondrial potential (AD = 10, control = 10). Mitochondrial depolarization is indicated by a decrease in the red/green fluorescence intensity ratio, while an increase reflects hyperpolarization. Additionally, the response of four cell subgroups to valinomycin, a potassium ionophore that induces mitochondrial depolarization, was measured.

To compare mitochondrial activity across the four cell subgroups, a two-way ANOVA with Tukey's test was conducted. For analyses within each cell type, we applied either a one-way ANOVA or a Kruskal–Wallis test, depending on the normality of the data. When comparing mitochondrial activity between AD and control groups, no significant differences were observed when all cell types were analyzed together, as shown in the Supplementary Fig. 7E-F. Further analysis of individual cell types revealed notable differences both among cell types and within each cell type when comparing AD and control groups (Suplementary Fig. 7 and Fig. 7B).

As shown in Fig. 7B, the JC-1 assay demonstrated significant differences in ΔΨm among the four cell subgroups. In AD, CD4 + cells exhibited significantly higher ΔΨm compared to CD8 + ($p = 0.0002$) and CD19 + cells ($p = 0.0009$). Similarly, CD14 + cells demonstrated increased ΔΨm compared to both CD19 + ($p = 0.0014$) and CD8 + cells ($p = 0.0003$).

When comparing AD and control groups within individual cell types, the JC-1 assay revealed a significant difference only in CD8 + cells, in which AD exhibited a higher ΔΨm compared to controls ($p = 0.02$) (Fig. 7B). No significant differences were observed in CD4 +, CD14 +, or CD19 + cells in these comparisons.

The JC-1 + valinomycin results showed that valinomycin induced mitochondrial depolarization in all cell groups except for CD8 + cells, where it caused an unexpected hyperpolarization (Fig. 7C). Additionally, the red/green ratio differences were used to calculate the responses of each cell type to valinomycin, as shown in the Supplementary Fig. 8. Notably, when comparing AD and control groups within each cell type, a significant difference was observed only in CD4 + cells, where AD samples exhibited higher levels of depolarization in response to valinomycin compared to controls ($p < 0.05$).

Discussion

AD is associated with immune system dysfunction, with pathological changes affecting both central and peripheral immune responses as the disease progresses[37]. T and B lymphocytes and monocytes play a key role in AD progression by engaging in diverse immune-driven mechanisms[37–40]. Understanding the diverse characteristics of peripheral immune cells in AD requires cell-specific studies[12,41]. While MS-based proteomic studies in AD have mostly focused on brain tissue and cerebrospinal fluid (CSF), blood-based analyses — especially in peripheral immune cells — remain largely underexplored, despite their potential to uncover novel biomarkers and insights into disease mechanisms[13,42–44]. Therefore, in this study, blood samples collected from AD patients and healthy donors were seperated into four peripheral immune cell groups —CD4 +, CD8 +, CD14 +, and CD19 +— using FACS, and comparative proteomic analysis was conducted within each immune cell type performed by LC–MS/MS.

Preliminary analysis showed no significant differences in CD14 + monocytes and CD19 + B cells, so further analyses were carried out with CD4 + and CD8 + T cells, which exhibited significant differences. Notably, the proteins significantly altered in these T cell subsets, involved in several pathways associated with AD, highlighting the complex structure of cellular responses. The hub proteins identified in both cell subgroups were closely associated with mitochondrial functions, emphasizing the critical role of mitochondrial dysfunction in the cellular processes contributing to disease development. This aligns with the growing evidence from previous research highlighting the importance of mitochondrial dysfunction in AD progression[9,10,19]. Although amyloid plaques are absent in peripheral tissues, mitochondrial dysfunction has been widely reported in peripheral cells of AD patients, including lymphocytes and platelets[45–47] Previous studies have documented increased oxidative stress, mitochondrial membrane potential changes, and metabolic abnormalities in systemic cells, supporting the idea of a peripheral bioenergetic signature of AD[48,49]. These alterations may be mediated by systemic inflammation, circulating amyloid-beta, or genetic risk factors such as APOE4[50,51]. Our results align with this body of work, highlighting cell-type-specific mitochondrial changes in peripheral T cells of AD patients. These findings suggest that mitochondrial dysfunction may serve as a shared pathological feature across central and peripheral compartments in AD.

Even though high number of proteins were revealed to be differentially expressed, our discussion will focus on hub proteins, which exhibited 1.5-fold or greater changes within the protein network in CD4 + and CD8 + T cells.

Bioinformatic analyses revealed that differentially expressed proteins in CD4 + cells were primarily enriched in RNA-binding and neurodegeneration-related pathways, whereas those in CD8 + cells were strongly associated with glycolytic metabolism and protein folding mechanisms. These findings suggest that AD-induced immune dysregulation involves multiple adaptive processes rather than a single pathway.

In CD4 + T cells, significant enrichment of ribosomal and spliceosome-associated proteins, implicate disruptions in RNA metabolism. Ribosomal proteins are known as targets for CD4 + T cells[52] and their presentation plays a crucial role in modulating immune responses[53]. Dysregulated ribosomal function is implicated in various diseases, including AD, where increased ribosomal complexes at the blood–brain barrier suggest a role in impaired protein processing in brain capillaries[54,55].

Our findings underscore the critical role of ribosomal proteins in AD progression. Among the 32 identified hub proteins, 20 were classified as ribosomal proteins. With the exception of RPL35A and RPS4X, expression levels of these 20 hub ribosomal proteins in the CD4 + T cells increased in AD patients.

When examining spliceosome-associated hub proteins, we identified that the RNA-binding proteins HNRNPA1, FUS, TDP-43, and HNRNPK exhibited significant changes in CD4 + T cells. Additionally, HNRNPA1 and HNRNPK were among the hub proteins. These proteins previously linked to neurodegeneration and investigated their involvement in oxidative stress responses[56–59]. Oxidative stress can cause these RNA-binding proteins to mislocalize from the nucleus to the cytoplasm, where they undergo post-translational modifications and aggregate within stress granules, contributing to neurodegenerative diseases[56–60]. Curdy et al.[61] demonstrated through proteomic and transcriptomic analyses that stress granules regulate immunological responses in activated T cells, with their findings significantly overlapping the hub proteins identified in CD4 + T cells in our study. RNA-binding proteins also interact with mitochondrial proteins and have important roles in mitochondrial functions[62]. HNRNPA1 promotes mitochondrial fragmentation by upregulating Drp1, while overexpressed TDP-43 disrupts mitochondrial-ER contacts, leading to mitochondrial deficits that drive a vicious cycle of oxidative damage and elevated ROS levels[59,62–66]. Our findings further support the relationship between RNA-binding protein dysregulation, mitochondrial dysfunction, and oxidative stress in AD. Significantly elevated ROS levels in CD4 + cells from AD patients were confirmed with MitoSOX Red assay. Furthermore, valinomycin induced significantly higher mitochondrial depolarization in the AD group. The relationship between proteomic differences and mitochondrial dysfunction highlights the role of oxidative stress and peripheral immune cell-specific functions in contributing to neurodegeneration in AD.

The majority of hub proteins in the CD8 + T cells are involved in glycolysis/gluconeogenesis metabolism and protein folding processes as mentioned before. We identified the HSPD1 protein, also known as HSP60, as a hub protein in CD8 + T cells, where it plays a role in mitochondrial chaperonin function and protein folding processes[67]. HSPD1 has been shown to interact with a variety of proteins involved in neurodegeneration, including FUS, which is linked to mitochondrial damage, as previously discussed[68]. HSPD1 levels in plasma and lymphocytes increased in the AD and MS groups compared to the control group[69,70]. In concordance with previous studies, we found that HSP60 levels are highly increased in CD8 + T cells in the AD group. It was also found that HSP90AA1 and HSP8 heat shock proteins are hub proteins in CD8 + T cells, which are also increased.

In addition to HSP proteins, we identified GLUD1 and MDH2 as hub mitochondrial proteins in CD8 + T cells, with their expression significantly elevated in the AD group. When examining other hub proteins, we observed elevated expression levels of GAPDH, PGK-1, PKM, and ENO2, which are directly involved in

glycolysis. Additionally, GAPDH, a glycolytic enzyme known to interact with multiple mitochondrial proteins, was identified as a hub protein with increased expression in both CD4 + and CD8 + T cells. A recent study on AD using CSF samples found increased expression of several ATP metabolism-related proteins, including MDH1 and ENO2[42]. This study highlighted the significance of dysfunction in energy metabolism and glycolytic alterations in the pathophysiology of the disease[42].

JC-1 assay results revealed a significant difference in ΔΨm specifically in CD8 + T cells. In the AD group, ΔΨm was hyperpolarized compared to the control group. Interestingly, we observed that this hyperpolarization persisted in CD8 + T cells despite the presence of valinomycin, distinguishing it from other cell subsets. The literature suggests that mitochondrial membrane hyperpolarization is associated with increased ROS levels and a metabolic shift towards glycolysis, driven by the upregulation of glycolytic enzymes in an oxidative environment[71–73]. While we did not observe a significant difference in ROS levels between AD and control groups within CD8 + T cells, we found that ROS levels were significantly higher in CD8 + T cells compared to CD4 + and CD19 + cells. Consistent with the relationship between hyperpolarization and glycolysis, our proteomic analysis revealed an upregulation of hub proteins associated with glycolysis/gluconeogenesis pathways in the CD8 + T cells. These findings align with the literature, and importantly, we demonstrate this relationship specifically in CD8 + T cells within the AD group, highlighting a cell-specific association between elevated glycolytic proteins and mitochondrial membrane hyperpolarization. The association of these increased glycolytic proteins and mitochondrial hyperpolarization in CD8 + T cells of AD patients further supports a metabolic reprogramming towards glycolysis.

Limitation

While APOE genotyping data were not available for the participants in this study, recent findings suggest that the APOE ε4 allele may influence PBMC proteomic profiles independently of AD status. Incorporating genotype-based stratification in future work could help further delineate subgroup-specific molecular patterns[74]. Similarly, although validated clinical tools such as the MMSE, CDR, and a comprehensive neuropsychological battery were employed to assess AD patients, the control group did not undergo formal cognitive evaluations. Nonetheless, control participants had no reported history or clinical signs of cognitive or mental health issues at the time of sampling and were not on neurological or psychiatric medications. This screening process likely reduced the risk of including individuals with unrecognized cognitive impairment, though the addition of standardized cognitive assessments would offer a more robust clinical context.

Conclusion

Our results emphasize the crucial part of peripheral immune cell dysregulation in AD, by showing mitochondrial and proteomic changes in CD4 + and CD8 + T cells. These changes underscore the importance of cell-specific studies in understanding the distinct immune mechanisms contributing to disease pathology.

In CD4 + T cells, observed expressional changes in ribosomal and RNA-binding proteins points to a disruption in RNA metabolism, which would help to explain increased ROS levels and mitochondrial dysfunction. In contrast, CD8 + T cells showed mitochondrial hyperpolarization and overexpression in glycolysis-related proteins, suggesting a metabolic shift towards glycolysis. Collectively, these results highlight a interplay between AD pathogenesis and the immune system changes, energy metabolism, oxidative stress, and mitochondrial dysfunction. By revealing critical hub proteins in CD4 + and CD8 + T cells and their related pathways, our study provides a valuable insights into the peripheral immune system's contributions to neurodegeneration. This study presents potential targets for future therapeutic approaches and modulating immune responses.

Data availability

The data generated and evaluated in this manuscript are included in the article and its supplementary materials.

Received: 30 April 2025; Accepted: 30 September 2025
Published online: 06 November 2025

References

1. Chen, M. et al. Common proteomic profiles of induced pluripotent stem cell-derived three-dimensional neurons and brain tissue from Alzheimer patients. *J. Proteom.* **182**, 21–33. https://doi.org/10.1016/j.jprot.2018.04.032 (2018).
2. Tsai, C. W. et al. An investigation of the correlation between the S-glutathionylated GAPDH levels in blood and Alzheimer's disease progression. *PLoS ONE* https://doi.org/10.1371/journal.pone.0233289 (2020).
3. Singh, C. S. B. et al. Conclusive demonstration of iatrogenic Alzheimer's disease transmission in a model of stem cell transplantation. *Stem Cell Rep.* **19**, 456–468. https://doi.org/10.1016/j.stemcr.2024.02.012 (2024).
4. Bu, X. L. et al. Blood-derived amyloid-β protein induces Alzheimer's disease pathologies. *Mol Psychiatry.* **23**, 1948–1956 (2018).
5. Hernandez, C. M. et al. Transfusion with Blood Plasma from Young Mice Affects rTg4510 Transgenic Tau Mice Modeling of Alzheimer's Disease. *Brain Sci.* **13**(6), 841. https://doi.org/10.3390/brainsci13060841 (2023).
6. Zhao, Y. et al. Young blood plasma reduces Alzheimer's disease-like brain pathologies and ameliorates cognitive impairment in 3×Tg-AD mice. *Alzheimers Res Ther.* **12**, 1–13 (2020).
7. Heneka, M. T., van der Flier, W. M., Jessen, F., Hoozemanns, J., Thal, D. R., Boche, D., et al. Neuroinflammation in Alzheimer disease. Nat. Rev. Immunol.. http://www.ncbi.nlm.nih.gov/pubmed/39653749 (2024).
8. Webers, A., Heneka, M. T. & Gleeson, P. A. The role of innate immune responses and neuroinflammation in amyloid accumulation and progression of Alzheimer's disease. *Immunol. Cell Biol.* **98**, 28–41. https://doi.org/10.1111/imcb.12301 (2020).
9. Misrani, A., Tabassum, S. & Yang, L. Mitochondrial Dysfunction and Oxidative Stress in Alzheimer's Disease. *Front. Aging Neurosci.* **13**, 1–20 (2021).
10. Song, T. et al. Mitochondrial dysfunction, oxidative stress, neuroinflammation, and metabolic alterations in the progression of Alzheimer's disease: A meta-analysis of in vivo magnetic resonance spectroscopy studies. *Ageing Res Rev.* **72**, 1–33 (2021).

11. Li, C. et al. Peripheral immune function and Alzheimer's disease: a living systematic review and critical appraisal. *Mol. Psychiatry* **29**, 1895–1905 (2024).
12. Xiong, L. L. et al. Single-cell RNA sequencing reveals B cell-related molecular biomarkers for Alzheimer's disease. *Exp. Mol. Med.* **53**, 1888–1901. https://doi.org/10.1038/s12276-021-00714-8 (2021).
13. Wang, H. et al. Integrated analysis of ultra-deep proteomes in cortex, cerebrospinal fluid and serum reveals a mitochondrial signature in Alzheimer's disease. *Mol. Neurodegener.* **15**, 1–20 (2020).
14. Whelan, C. D. et al. Multiplex proteomics identifies novel CSF and plasma biomarkers of early Alzheimer's disease. *Acta Neuropathol. Commun.* **7**, 1–14 (2019).
15. Thambisetty, M. et al. Proteome-based plasma markers of brain amyloid-β deposition in non-demented older individuals. *J. Alzheimer's Dis.* **22**, 1099–1109 (2010).
16. Yu, H., Liu, Y., He, B., He, T., Chen, C., He, J., et al. Platelet biomarkers for a descending cognitive function: A proteomic approach. Aging Cell. [cited 2022 Jan 4] 20. https://pubmed.ncbi.nlm.nih.gov/33942972/ (2021).
17. Bhatia, S. et al. Mitochondrial Dysfunction in Alzheimer's Disease: Opportunities for Drug Development. *Curr. Neuropharmacol.* **20**, 675–692 (2021).
18. Apaijai, N. et al. Cognitive impairment is associated with mitochondrial dysfunction in peripheral blood mononuclear cells of elderly population. *Sci. Rep.* **10**, 1–8. https://doi.org/10.1038/s41598-020-78551-4 (2020).
19. Sultana, M. A., Hia, R. A., Akinsiku, O. & Hegde, V. Peripheral Mitochondrial Dysfunction: A Potential Contributor to the Development of Metabolic Disorders and Alzheimer's Disease. *Biology (Basel).* **12**(7), 1019. https://doi.org/10.3390/biology12071019 (2023).
20. Smith, A. M. et al. Mitochondrial dysfunction and increased glycolysis in prodromal and early Parkinson's blood cells. *Mov. Disord.* **33**, 1580–1590 (2018).
21. McKhann, G. et al. Clinical diagnosis of Alzheimer's disease: report of the NINCDS-ADRDA Work Group under the auspices of Department of Health and Human Services Task Force on Alzheimer's Disease. *Neurology* **34**, 939–944 (1984).
22. Morris, J. C. The Clinical Dementia Rating (CDR): current version and scoring rules. *Neurology* **43**, 2412–2414 (1993).
23. Folstein, M. F., Robins, L. N. & Helzer, J. E. The Mini-Mental State Examination. *Arch. Gen. Psychiatry* **40**, 812. https://doi.org/10.1001/archpsyc.1983.01790060110016 (1983).
24. Kiris, I. et al. Evaluation of the Therapeutic Effect of Lycoramine on Alzheimer's Disease in Mouse Model. *Curr. Med. Chem.* **28**, 3449–3473 (2020).
25. Valero-Mora, P. M. ggplot2: Elegant Graphics for Data Analysis. In *J Stat Softw* (ed. Wickham, H.) 189–201 (Cham: Springer International Publishing, 2010). https://doi.org/10.1007/978-3-319-24277-4_9.
26. Ashburner, M. et al. Gene Ontology: tool for the unification of biology. *Nat. Genet.* **25**, 25–29. https://doi.org/10.1038/75556 (2000).
27. Kanehisa, M. & Goto, S. KEGG: kyoto encyclopedia of genes and genomes. *Nucleic Acids Res.* **28**, 27–30 (2000).
28. Walter, W., Sánchez-Cabo, F. & Ricote, M. GOplot: an R package for visually combining expression data with functional analysis. *Bioinformatics* **31**, 2912–2914 (2015).
29. Kanehisa, M., Furumichi, M., Sato, Y., Matsuura, Y. & Ishiguro-Watanabe, M. KEGG: biological systems database as a model of the real world. *Nucleic Acids Res.* **53**, D672–D677 (2025).
30. Szklarczyk, D. et al. The STRING database in 2017: quality-controlled protein–protein association networks, made broadly accessible. *Nucleic Acids Res.* **45**, D362–D368. https://doi.org/10.1093/nar/gkw937 (2017).
31. Shannon, P. et al. Cytoscape: a software environment for integrated models of biomolecular interaction networks. *Genome Res.* **13**, 2498–2504 (2003).
32. Chin, C. H. et al. cytoHubba: identifying hub objects and sub-networks from complex interactome. *BMC Syst. Biol.* **8**, S11. https://doi.org/10.1186/1752-0509-8-S4-S11 (2014).
33. Legeay, M., Doncheva, N. T., Morris, J. H. & Jensen, L. J. Visualize omics data on networks with Omics Visualizer, a Cytoscape App. *F1000Res* **9**, 157 (2020).
34. Bindea, G. et al. ClueGO: a Cytoscape plug-in to decipher functionally grouped gene ontology and pathway annotation networks. *Bioinformatics* **25**, 1091–1093. https://doi.org/10.1093/bioinformatics/btp101 (2009).
35. Smiley, S. T. et al. Intracellular heterogeneity in mitochondrial membrane potentials revealed by a J-aggregate-forming lipophilic cation JC-1. *Proc. Natl. Acad.. Sci. U. S. A.* **88**, 3671–3675 (1991).
36. Perelman, A. et al. JC-1: Alternative excitation wavelengths facilitate mitochondrial membrane potential cytometry. *Cell Death Dis.* **3**, e430–e437. https://doi.org/10.1038/cddis.2012.171 (2012).
37. Bettcher BM, Tansey MG, Dorothée G, Heneka MT. Peripheral and central immune system crosstalk in Alzheimer disease — a research prospectus. Nature Reviews Neurology 2021 17:11 [Internet]. [cited 2022 Jan 6];17:689–701. https://www.nature.com/articles/s41582-021-00549-x (2021).
38. Rossi, B., Santos-Lima, B., Terrabuio, E., Zenaro, E. & Constantin, G. Common Peripheral Immunity Mechanisms in Multiple Sclerosis and Alzheimer's Disease. *Front. Immunol.* **12**, 404 (2021).
39. Qian XH, Liu XL, Chen S Di, Tang HD. Integrating peripheral blood and brain transcriptomics to identify immunological features associated with Alzheimer's disease in mild cognitive impairment patients. Front Immunol. [cited 2023 Jan 25];13. /pmc/articles/PMC9501700/ (2022).
40. Heneka, M. T. et al. Neuroinflammation in Alzheimer's Disease. *Lancet Neurol.* **14**, 388 (2015).
41. Phongpreecha, T. et al. Single-cell peripheral immunoprofiling of Alzheimer's and Parkinson's diseases. *Sci. Adv.* https://doi.org/10.1126/sciadv.abd5575 (2020).
42. Pichet Binette, A. et al. Proteomic changes in Alzheimer disease associated with progressive Aβ plaque and tau tangle pathologies. *Nat. Neurosci.* https://doi.org/10.1038/s41593-024-01737-w (2024).
43. Bai, B. et al. Proteomic landscape of Alzheimer's Disease: novel insights into pathogenesis and biomarker discovery. *Mol. Neurodegener.* **16**, 1–16 (2021).
44. Rehiman, S. H. et al. Proteomics as a reliable approach for discovery of blood-based Alzheimer's disease biomarkers: A systematic review and meta-analysis. *Ageing Res. Rev.* https://doi.org/10.1016/j.arr.2020.101066 (2020).
45. Coskun, P. E. et al. Systemic mitochondrial dysfunction and the etiology of Alzheimer's disease and down syndrome dementia. *J. Alzheimers Dis.* **20**(Suppl 2), S293-310 (2010).
46. Keskinoz, E. N. et al. Mitochondrial Alterations in Alzheimer's Disease: Insight from the 5xFAD Mouse Model. *Mol. Neurobiol.* **62**, 7075–7092. https://doi.org/10.1007/s12035-024-04632-4 (2025).
47. Leuner, K. et al. Peripheral mitochondrial dysfunction in Alzheimer's disease: Focus on lymphocytes. *Mol. Neurobiol.* **46**, 194–204 (2012).
48. Cortes, C. J., Thyfault, J. P. & Wilkins, H. M. Editorial: Systemic implications of Alzheimer's disease. *Front. Aging Neurosci.* https://doi.org/10.3389/fnagi.2023.1219987 (2023).
49. Fanlo-Ucar H, Picón-Pagès P, Herrera-Fernández V, ILL-Raga G, Muñoz FJ. The Dual Role of Amyloid Beta-Peptide in Oxidative Stress and Inflammation: Unveiling Their Connections in Alzheimer's Disease Etiopathology. Antioxidants. 13. https://www.mdpi.com/2076-3921/13/10/1208 (2024).
50. Juul-Madsen, K. et al. Amyloid-β aggregates activate peripheral monocytes in mild cognitive impairment. *Nat. Commun.* **15**, 1224. https://doi.org/10.1038/s41467-024-45627-y (2024).

51. Swerdlow, R. H. Mitochondria and Mitochondrial Cascades in Alzheimer's Disease. *J. Alzheimer's Dis.* **62**, 1403–1416. https://doi.org/10.3233/JAD-170585 (2018).
52. Kennedy, S. C. et al. Identification of Mycobacterial Ribosomal Proteins as Targets for CD4^{+}T Cells That Enhance Protective Immunity in Tuberculosis. *Infect. Immun.* https://doi.org/10.1128/iai.00009-18 (2018).
53. Philip, M., Schietinger, A. & Schreiber, H. Ribosomal versus non-ribosomal cellular antigens: factors determining efficiency of indirect presentation to CD4+T cells. *Immunology* **130**, 494–503. https://doi.org/10.1111/j.1365-2567.2010.03258.x (2010).
54. Jiao, L. et al. Ribosome biogenesis in disease: new players and therapeutic targets. *Signal Trans. Targeted Ther.* **8**, 1–22 (2023).
55. Suzuki, M. et al. Upregulation of ribosome complexes at the blood-brain barrier in Alzheimer's disease patients. *J. Cereb. Blood Flow Metab.* **42**, 2134–2150 (2022).
56. Clarke, J. P., Thibault, P. A., Salapa, H. E. & Levin, M. C. A Comprehensive Analysis of the Role of hnRNP A1 Function and Dysfunction in the Pathogenesis of Neurodegenerative Disease. *Front. Mol. Biosci.* **8**, 1–19 (2021).
57. Salapa, H. E. et al. hnRNP A1 dysfunction alters RNA splicing and drives neurodegeneration in multiple sclerosis (MS). *Nat. Commun.* **15**, 1–19 (2024).
58. Bampton, A. et al. HnRNP K mislocalisation is a novel protein pathology of frontotemporal lobar degeneration and ageing and leads to cryptic splicing. *Acta Neuropathol.* **142**, 609–627. https://doi.org/10.1007/s00401-021-02340-0 (2021).
59. Harley, J., Clarke, B. E. & Patani, R. The interplay of rna binding proteins, oxidative stress and mitochondrial dysfunction in als. *Antioxidants.* **10**(4), 552. https://doi.org/10.3390/antiox10040552 (2021).
60. Salapa, H. E., Libner, C. D. & Levin, M. C. Dysfunctional RNA-binding protein biology and neurodegeneration in experimental autoimmune encephalomyelitis in female mice. *J. Neurosci. Res.* **98**, 704–717 (2020).
61. Curdy, N., Lanvin, O., Cerapio, J. P., Pont, F., Tosolini, M., Sarot, E., et al. The proteome and transcriptome of stress granules and P bodies during human T lymphocyte activation. Cell Rep. 42. (2023).
62. Zuo, X. et al. TDP-43 aggregation induced by oxidative stress causes global mitochondrial imbalance in ALS. *Nat. Struct. Mol. Biol.* **28**, 132–142. https://doi.org/10.1038/s41594-020-00537-7 (2021).
63. Park, S. J. et al. Heterogeneous nuclear ribonucleoprotein A1 post-transcriptionally regulates Drp1 expression in neuroblastoma cells. *Biochim. Biophys. Acta Gene Regul. Mech.* **1849**, 1423–1431. https://doi.org/10.1016/j.bbagrm.2015.10.017 (2015).
64. Briese, M. et al. Loss of Tdp-43 disrupts the axonal transcriptome of motoneurons accompanied by impaired axonal translation and mitochondria function. *Acta Neuropathol. Commun.* **8**, 1–16 (2020).
65. Gautam, M. et al. Mitochondria, ER, and nuclear membrane defects reveal early mechanisms for upper motor neuron vulnerability with respect to TDP-43 pathology. *Acta Neuropathol.* **137**, 47–69. https://doi.org/10.1007/s00401-018-1934-8 (2019).
66. Wang P, Deng J, Dong J, Liu J, Bigio EH, Mesulam M, et al. TDP-43 induces mitochondrial damage and activates the mitochondrial unfolded protein response. PLoS Genet. (2019).
67. Morgenstern, M. et al. Quantitative high-confidence human mitochondrial proteome and its dynamics in cellular context. *Cell Metab.* **33**, 2464-2483.e18 (2021).
68. Deng, J. et al. FUS Interacts with HSP60 to Promote Mitochondrial Damage. *PLoS Genet.* **11**, e1005357. https://doi.org/10.1371/journal.pgen.1005357 (2015).
69. Marino Gammazza, A. et al. Circulating Molecular Chaperones in Subjects with Amnestic Mild Cognitive Impairment and Alzheimer's Disease: Data from the Zabùt Aging Project. *J. Alzheimer's Dis.* **87**, 161–172. https://doi.org/10.3233/JAD-180825 (2022).
70. Pennisi, G. et al. Redox regulation of cellular stress response in multiple sclerosis. *Biochem. Pharmacol.* **82**, 1490–1499. https://doi.org/10.1016/j.bcp.2011.07.092 (2011).
71. Sánchez-Villanueva, J. A. et al. Contribution of ROS and metabolic status to neonatal and adult CD8+ T cell activation. *PLoS ONE* **14**, e0226388. https://doi.org/10.1371/journal.pone.0226388 (2019).
72. Henson, S. M. et al. p38 signaling inhibits mTORC1-independent autophagy in senescent human CD8+ T cells. *J. Clin. Invest.* **124**, 4004–4016 (2014).
73. Akkaya, B. et al. Increased Mitochondrial Biogenesis and Reactive Oxygen Species Production Accompany Prolonged CD4+ T Cell Activation. *J. Immunol.* **201**, 3294–3306 (2018).
74. Philippi, S. M., Kailash, B. P., Raj, T. & Castellano, J. M. APOE genotype and brain amyloid are associated with changes in the plasma proteome in elderly subjects without dementia. *Ann. Clin. Transl. Neurol.* **12**, 366–382 (2025).

Acknowledgements

We would like to thank Assist. Prof. Dr. Nur Mustafaoglu from Sabanci University for her valuable support in the preparation of scientific illustrations.

Author contributions

Conceptualization: S.K., A.T.B.; Methodology: S.K., A.T.B.; Validation: SK; Formal Analysis: S.K.; Investigation: S.K.; Writing – Original Draft: S.K.; Review & Editing: S.K., I.K.; Visualization: S.K., I.K.; Resources: S.S., N.C., S.Ka.; Supervision: A.T.B.; Project Administration: A.T.B.; Funding Acquisition: A.T.B.

Funding

This study was supported by TUBITAK (Scientific and Technological Research Council of Turkey) (Project Number: 216S605).

Declarations

Competing interests

The authors declare no competing interests.

Ethical approval

The research was approved by the Clinical Research Ethics Committee (ATADEK) at Acibadem Mehmet Ali Aydinlar University (No: 2016/8–34, Date: 12 May 2016) and complies with the guidelines of the Helsinki Declaration. A written informed consent was given by all participants who took part in this study.

Additional information

Supplementary Information The online version contains supplementary material available at https://doi.org/10.1038/s41598-025-22783-9.

Correspondence and requests for materials should be addressed to A.T.B.